



Plasma and thermoforming treatments to tune the bio-inspired wettability of polystyrene

E. Lepore^a, P. Faraldi^b, D. Bongini^b, L. Boarino^c, N. Pugno^{a,c,d,*}

^a Laboratory of Bio-inspired Nanomechanics “Giuseppe Maria Pugno”, Department of Structural Engineering, Politecnico di Torino, Corso Duca degli Abruzzi 24, 10129 Torino, Italy

^b Indesit Company, Viale Aristide Merloni 47, 60044 Fabriano (AN), Italy

^c National Institute of Metrological Research, Strada delle Cacce 91, 10135 Torino, Italy

^d National Institute of Nuclear Physics, National Laboratories of Frascati, Via E. Fermi 40, 00044 Frascati, Italy

ARTICLE INFO

Article history:

Received 16 November 2010
Received in revised form 19 January 2011
Accepted 17 May 2011
Available online 23 May 2011

Keywords:

A. Nano-structures
A. Smart materials
B. Wettability
D. Surface analysis
Lotus

ABSTRACT

This paper shows the effects on wettability of plasma and thermoforming treatments on 14 different polystyrene (PS) surfaces, with a comparison with a lotus leaf. Quantitative roughness analyses of PS surfaces and lotus leaf, by three-dimensional optical profilometer and scanning electron microscope, have been carried out. We characterized the water drop sliding by measuring the contact angle, sliding angle, sliding volume and sliding speed. A relevant correlation between technological treatment, surface roughness parameters and wetting measurements clearly emerges, suggesting the plasma/thermoforming treatment as a process for enhancing the hydrophilic/hydrophobic behavior of PS surfaces. Determination of the static and resistant forces of the drop sliding on the surfaces concludes the paper.

© 2011 Elsevier Ltd. All rights reserved.

1. Introduction

Water-repellent (or super-hydrophobic) and dirt-free (or self-cleaning) natural surfaces were probably observed for the first time more than 2000 years ago; however, only in the 20th century scientists studied these two related phenomena on some natural leaves [1–10], e.g. the famous lotus *Nelumbo nucifera*, on which “raindrops take a clear, spherical shape without spreading, which probably has to be ascribed to some kind of evaporated essence”, as Goethe described in 1817 [11].

In contrast to the Goethe’s conjecture, the so called lotus-effect is governed more than by chemistry (Young’s law [12]) by topology (Wenzel’s law [13], Cassie–Baxter’s law [14]) and hierarchical architectures [15,16] (similar to what we observe on the strength and toughness of materials [17–21]). The contribution of surface roughness on super-hydrophobic/self-cleaning behavior has been extensively shown in the literature [22–34]. However, in some applications, materials should be hydrophilic more than hydrophobic, e.g. in order to maximize wettability.

In this paper, we study the effects of plasma or thermoforming treatments on different polystyrene (PS) surfaces. We have consid-

ered seven PS surfaces before (A_p) or after (B_p) the plasma treatment and fourteen PS surfaces before (A_t) or after (B_t) the thermoforming treatment. All these surfaces have been analysed with a three-dimensional optical profilometer and a field emission scanning electron microscope. The hydrophilic behavior given by plasma treatment is quantified by depositing distilled water drops on PS horizontal surfaces with controlled or random volumes, showing a relevant correlation between surface roughness parameters and contact angles (CA) measurements, in accordance with Wenzel theory. The effects of the thermoforming treatment are quantified by measuring the drop contact angle, sliding angle, volume and speed. Finally, we determine the static and resistant forces of a drop sliding on the surfaces.

2. Materials and methods

2.1. Plasma treatment

A commonly applied method to increase wettability and chemical reactivity of polymeric materials (by raising surface energy) is plasma discharge treatment, also known as corona treatment. Such treatment, invented by the Danish engineer Verner Eisby in the 1950s, is particularly suitable for continuous production processes, like the extruded PS sheets constituting the subject of the present paper, being safe, economical and capable of high line speed throughput.

* Corresponding author at: Laboratory of Bio-inspired Nanomechanics “Giuseppe Maria Pugno”, Department of Structural Engineering, Politecnico di Torino, Corso Duca degli Abruzzi 24, 10129 Torino, Italy. Tel.: +39 011 564 4902; fax: +39 011 564 4899.

E-mail address: nicola.pugno@polito.it (N. Pugno).

Table 1
Measured roughness parameters of all PS surfaces. Note that samples 7A_p and 7B_p are used only to evaluate the effects of plasma treatment, while 7A_t and 14A_t are new samples for the determination of the effects of thermoforming treatment.

| | Sa (μm) | Sq (μm) | Sp (μm) | Sv (μm) | Sz (μm) | Ssk | Sdr (%) |
|------------------------------------|----------------|----------------|------------------|-----------------|------------------|-----------------|-----------------|
| 1A _p = 1A _t | 0.671 ± 0.0142 | 0.859 ± 0.0165 | 4.267 ± 0.3092 | 5.340 ± 1.2821 | 8.240 ± 0.6894 | -0.274 ± 0.0118 | 5.583 ± 0.1041 |
| 2A _p = 2A _t | 0.753 ± 0.0490 | 0.970 ± 0.0603 | 4.697 ± 0.9258 | 6.027 ± 0.1950 | 8.967 ± 0.3204 | -0.136 ± 0.0431 | 5.277 ± 0.2930 |
| 3A _p = 3A _t | 0.205 ± 0.0062 | 0.266 ± 0.0036 | 1.907 ± 1.0249 | 1.803 ± 0.5505 | 2.790 ± 0.6490 | 0.217 ± 0.1808 | 0.273 ± 0.0356 |
| 4A _p = 4A _t | 0.086 ± 0.0093 | 0.126 ± 0.0162 | 2.160 ± 0.6907 | 1.863 ± 0.8615 | 2.833 ± 0.5776 | 0.821 ± 0.0993 | 0.108 ± 0.0242 |
| 5A _p = 5A _t | 1.197 ± 0.1201 | 2.143 ± 0.1589 | 11.500 ± 1.1790 | 16.500 ± 1.9698 | 24.867 ± 0.7234 | -2.523 ± 0.4826 | 11.003 ± 1.7306 |
| 6A _p = 6A _t | 0.120 ± 0.0178 | 0.156 ± 0.0246 | 1.201 ± 0.3090 | 0.896 ± 0.1965 | 1.530 ± 0.3989 | 0.138 ± 0.1238 | 0.060 ± 0.0224 |
| 7A _t | 0.744 ± 0.0840 | 0.946 ± 0.1150 | 3.553 ± 1.7032 | 4.613 ± 0.6638 | 6.01 ± 0.8402 | -0.444 ± 0.1785 | 0.486 ± 0.0927 |
| 1B _p = 8A _t | 1.730 ± 0.0954 | 2.203 ± 0.1250 | 12.963 ± 5.7969 | 13.927 ± 6.9070 | 21.300 ± 3.8626 | -0.074 ± 0.1316 | 20.800 ± 1.3454 |
| 2B _p = 9A _t | 1.330 ± 0.0557 | 1.693 ± 0.0777 | 6.960 ± 0.2598 | 9.353 ± 1.0207 | 14.167 ± 0.8083 | -0.144 ± 0.1593 | 14.500 ± 0.7937 |
| 3B _p = 10A _t | 0.921 ± 0.0093 | 1.187 ± 0.0115 | 4.403 ± 0.1950 | 6.657 ± 0.4466 | 10.080 ± 0.4703 | -0.331 ± 0.0999 | 7.090 ± 0.1572 |
| 4B _p = 11A _t | 1.427 ± 0.0681 | 1.857 ± 0.0751 | 8.747 ± 0.4735 | 9.780 ± 0.1212 | 16.400 ± 0.6000 | -0.383 ± 0.1866 | 12.967 ± 0.9292 |
| 5B _p = 12A _t | 0.939 ± 0.0302 | 1.213 ± 0.0351 | 5.627 ± 1.1371 | 6.733 ± 1.2595 | 10.473 ± 1.0403 | -0.289 ± 0.2050 | 6.293 ± 0.7801 |
| 6B _p = 13A _t | 1.273 ± 0.1361 | 1.653 ± 0.1818 | 6.657 ± 0.6311 | 9.553 ± 0.6243 | 14.367 ± 0.9238 | -0.396 ± 0.1102 | 11.663 ± 1.8067 |
| 14A _t | 0.745 ± 0.1322 | 0.953 ± 0.1662 | 4.555 ± 0.9122 | 4.425 ± 1.3647 | 6.365 ± 0.5020 | -0.171 ± 0.0643 | 0.617 ± 0.0573 |
| 7A _p | 0.313 ± 0.0159 | 0.403 ± 0.0232 | 2.647 ± 0.8939 | 2.383 ± 0.3646 | 3.913 ± 0.6824 | 0.076 ± 0.1178 | 0.629 ± 0.1203 |
| 7B _p | 1.427 ± 0.1762 | 1.867 ± 0.2444 | 20.757 ± 17.4233 | 11.333 ± 0.7506 | 24.767 ± 11.8289 | -0.306 ± 0.4491 | 15.533 ± 3.0600 |
| 1B _t | 0.841 ± 0.2010 | 1.059 ± 0.2403 | 3.443 ± 1.3640 | 3.970 ± 0.2600 | 5.827 ± 1.0645 | -0.276 ± 0.1651 | 0.572 ± 0.2196 |
| 2B _t | 0.647 ± 0.0785 | 0.827 ± 0.0960 | 3.910 ± 1.2305 | 4.187 ± 2.0814 | 4.870 ± 0.3477 | -0.128 ± 0.1611 | 0.373 ± 0.0810 |
| 3B _t | 0.675 ± 0.0642 | 0.856 ± 0.0711 | 2.660 ± 0.5467 | 3.320 ± 0.3329 | 5.147 ± 0.3156 | -0.242 ± 0.0804 | 0.401 ± 0.0201 |
| 4B _t | 0.235 ± 0.0115 | 0.298 ± 0.0141 | 1.250 ± 0.0889 | 1.590 ± 0.5597 | 1.850 ± 0.0624 | 0.265 ± 0.2493 | 0.048 ± 0.0088 |
| 5B _t | 0.359 ± 0.0654 | 0.463 ± 0.0883 | 2.020 ± 0.7544 | 2.020 ± 0.3724 | 2.837 ± 0.7211 | -0.326 ± 0.1570 | 0.101 ± 0.0299 |
| 6B _t | 0.518 ± 0.0474 | 0.644 ± 0.0551 | 2.123 ± 0.3204 | 2.553 ± 0.1701 | 3.757 ± 0.3988 | -0.026 ± 0.0123 | 0.228 ± 0.0653 |
| 7B _t | 0.602 ± 0.0762 | 0.757 ± 0.0993 | 2.917 ± 0.8153 | 3.133 ± 0.7427 | 4.413 ± 0.4332 | -0.095 ± 0.1010 | 0.342 ± 0.0898 |
| 8B _t | 0.933 ± 0.905 | 1.180 ± 0.1414 | 5.690 ± 0.2121 | 4.460 ± 1.3435 | 6.580 ± 0.8768 | -0.044 ± 0.1061 | 0.724 ± 0.2531 |
| 9B _t | 0.528 ± 0.0240 | 0.672 ± 0.0212 | 2.335 ± 0.0071 | 2.605 ± 0.6718 | 4.130 ± 0.1131 | 0.166 ± 0.0938 | 0.261 ± 0.0078 |
| 10B _t | 0.384 ± 0.0643 | 0.476 ± 0.0813 | 2.815 ± 1.9304 | 1.630 ± 0.1980 | 2.695 ± 0.2333 | 0.061 ± 0.0016 | 0.103 ± 0.0160 |
| 11B _t | 0.545 ± 0.0750 | 0.700 ± 0.1103 | 2.485 ± 0.5869 | 2.645 ± 0.6010 | 4.610 ± 1.1031 | -0.023 ± 0.0629 | 0.368 ± 0.1697 |
| 12B _t | 0.466 ± 0.0566 | 0.588 ± 0.0636 | 2.085 ± 0.0495 | 2.295 ± 0.1626 | 3.695 ± 0.0919 | -0.006 ± 0.0991 | 0.214 ± 0.0078 |
| 13B _t | 0.113 ± 0.0085 | 0.147 ± 0.0007 | 0.739 ± 0.3974 | 0.518 ± 0.0007 | 0.955 ± 0.1344 | 0.444 ± 0.6678 | 0.018 ± 0.0003 |
| 14B _t | 0.616 ± 0.0827 | 0.786 ± 0.1209 | 3.010 ± 0.7637 | 3.275 ± 0.8697 | 4.605 ± 1.0112 | 0.018 ± 0.2737 | 0.336 ± 0.0849 |

Corona treatment is based on a high-frequency and high-voltage electrical discharge. The discharge is generated between an electrode and a counter electrode. The corona discharge has such a powerful impact on the substance surface that the molecular structure changes in a way that improves the surface wettability. In the presence of a high voltage discharge in an air gap, air ionization occurs. If a plastic material is placed in the discharge path, the electrons generated in the discharge impact the surface with energies two or three times larger than that necessary to break the molecular bonds. This creates very reactive free radicals that, in presence of air oxygen, can react rapidly to form various chemical functional groups on the substrate surface. An evolution of the system, particularly efficient for the higher activation potential, is the plasma jet system, where by means of high-voltage discharge (5–15 kV, 10–100 kHz) a pulsed electric arc is generated. A process gas, usually oil-free compressed air flowing past this discharge section, is excited and converted to the plasma state. This plasma then passes through a jet head to arrive on the surface of the material to be treated. The jet head is at earth potential and in this way largely holds back potential-carrying parts of the plasma stream. Corona surface and plasma jet treatment modifies only the surface characteristics without affecting material bulk properties [35–37].

Corona discharge treatment is commonly applied in cooling appliance industry: refrigerator insulation systems are typically constituted by polyurethane foam, reticulated *in situ* within cavity designed by purpose. To ensure mechanical and thermal stability of the final assembly, and thanks to the strongly modified surface topology due to the plasma treatment, adhesion of polyurethane foam over surrounding surfaces, i.e. PS liner surface and external case, must be maximized. For the purposes of the present paper, PS extruded slabs have been treated with the industrial “Ferrarini and Benelli” corona discharge system, integrated within refrigerators production line at Indesit Company; main characteristics of the equipment are: nominal power (7.3 kVA), corona discharge

power (6.5 kW), corona discharge device working frequency (30 kHz), achievable surface energy after treatment $((4.2–5.6) \times 10^{-2} \text{ N/m})$, material temperature in treatment area (80 °C), performance test method (ASTM Standard Test Method D2578–84, “Wetting Tension of Polyethylene and Polypropylene Film”).

2.2. Thermoforming treatment

Thermoforming is the technology almost universally applied for refrigerator cabinet liner and door internal surface manufacturing; such technique allows high throughput production, together with a very good net shape surface finishing. Main phases of the process are: pre-heating (100 °C), peak temperature (180 °C), final temperature (70 °C).

After thermoforming, thickness reduction can exceed 90% in some areas: a careful control is needed to verify that sheet is kept robust (e.g. no breakage of aesthetic or functional layer), tuning the process and the material characteristics.

2.3. Surface characterization

The characterization of PS surfaces was performed with a three-dimensional optical profilometer, Talysurf CLI 1000, equipped with the CLA Confocal Gauge 300HE or a mechanical cantilever with 300 μm range and 10 nm vertical resolution or with 546 μm range and 10 nm vertical resolution from Taylor Hobson, Leicester, UK. The parameters tuned during the analysis are the measurement speed equal to 200 μm/s, the return speed equal to 1 mm/s or 500 μm/s, the sampling rate equal to 150 Hz or 40 Hz, the measured area equal to 500 × 500 μm² and the resolution in the “xy” plane equal to 2.5 μm, leading to a final resolution of 201 points/profile. All parameters were referred to a 250 μm cut-off. See [38–40] for a detailed explanation of the classical roughness parameters extracted (Sa, Sq, Sp, Sv, Sz, Ssk, Sdr).

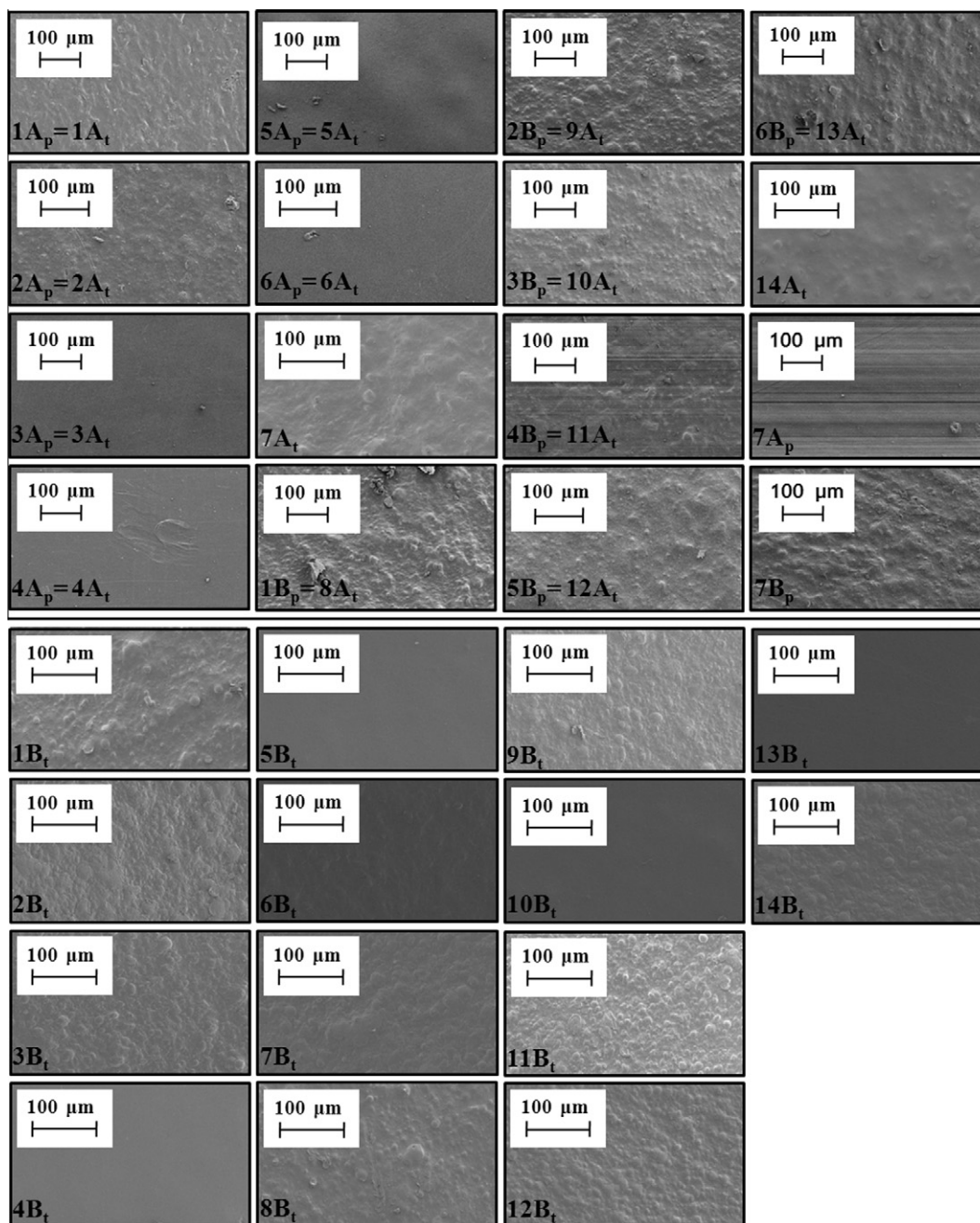


Fig. 1. FESEM microscopies of the tested PS surfaces.

We also observed the PS surfaces and lotus leaf by means of a field emission scanning electron microscope (FESEM, ZEISS SUPRA 40 for A_p , B_p and A_t samples and lotus leaf, or FEI-Inspect™ F50 for B_t samples) equipped with a field emission tungsten cathode. Samples of $\sim 1 \text{ cm}^2$ were obtained, fixed to aluminum stubs by double-sided adhesive carbon conductive tape (Nisshin EM Co. Ltd.), ethanol-cleaned (except for lotus leaf used as is) and air-dried. Samples A_p , B_p and lotus leaf or A_t and B_t were chrome or gold-coated, approximately 8 or 3.6 nm.

2.4. CA measurement

The wettability of PS surfaces and lotus leaf was determined by measuring the static CA of distilled water droplets over the samples, fixed to a horizontal plane by a double-sided adhesive tape and cleaned with ethanol before drop deposition, in order

to reduce the negative influence of sample cleanliness on contact angle measurements [41–44]. We consider a series of 10 random-volume drops, gently deposited on the substrate with a standard single use syringe, and nine controlled-volume drops (0.5, 0.7, 0.9, 1.1, 1.3, 1.5, 1.7, 1.9, 2.0 μl), deposited with a digital micropipette (Gilson, Ultra-range U2-Model, 0.2–2.0 μl). The contact angle was recorded with an OLYMPUS MJU 1010 digital photo-camera, measured and statistically analysed with the software ImageJ 1.41o.

2.5. Sliding measurements

Two conceptually distinct procedures were used to evaluate the sliding angles on B_t samples and lotus leaf: (1) fixing the volume ($\sim 16 \mu\text{l}$) and measuring the angle at sliding or (2) fixing the angle (90°) and measuring the sliding volume.

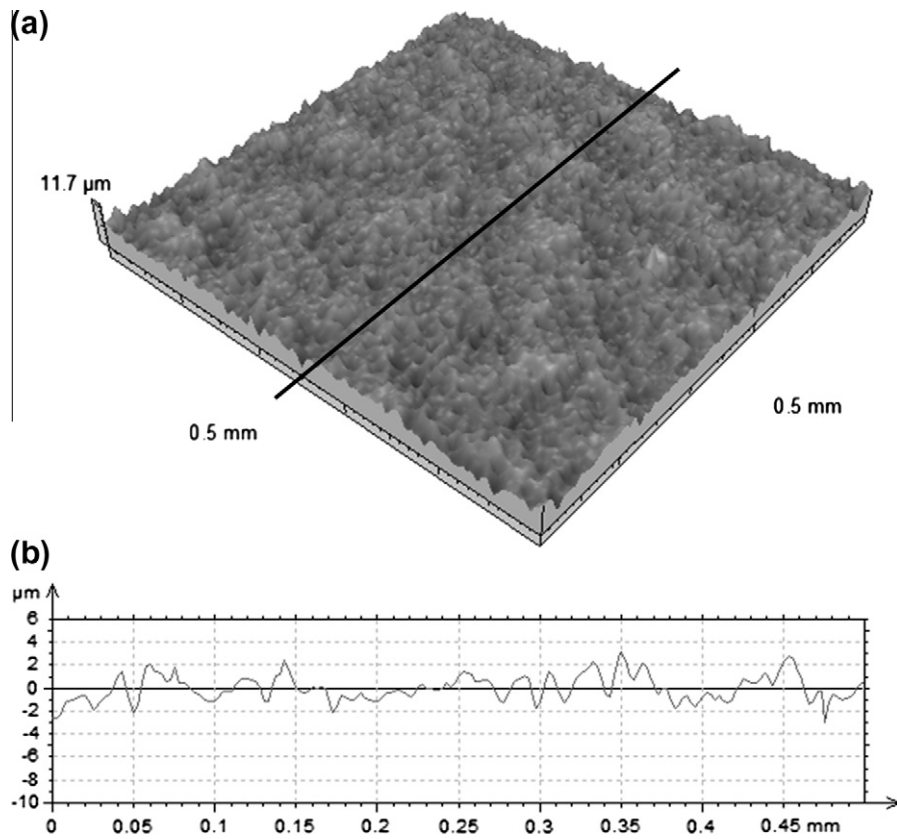


Fig. 2. Surface topography before plasma treatment. PS surface of sample 2A_p, as representative of surface topography of samples 1A_p and 2A_p. (a) 3D topography and (b) 2D profile (extracted at 50 mm from the edge of the square measured area).

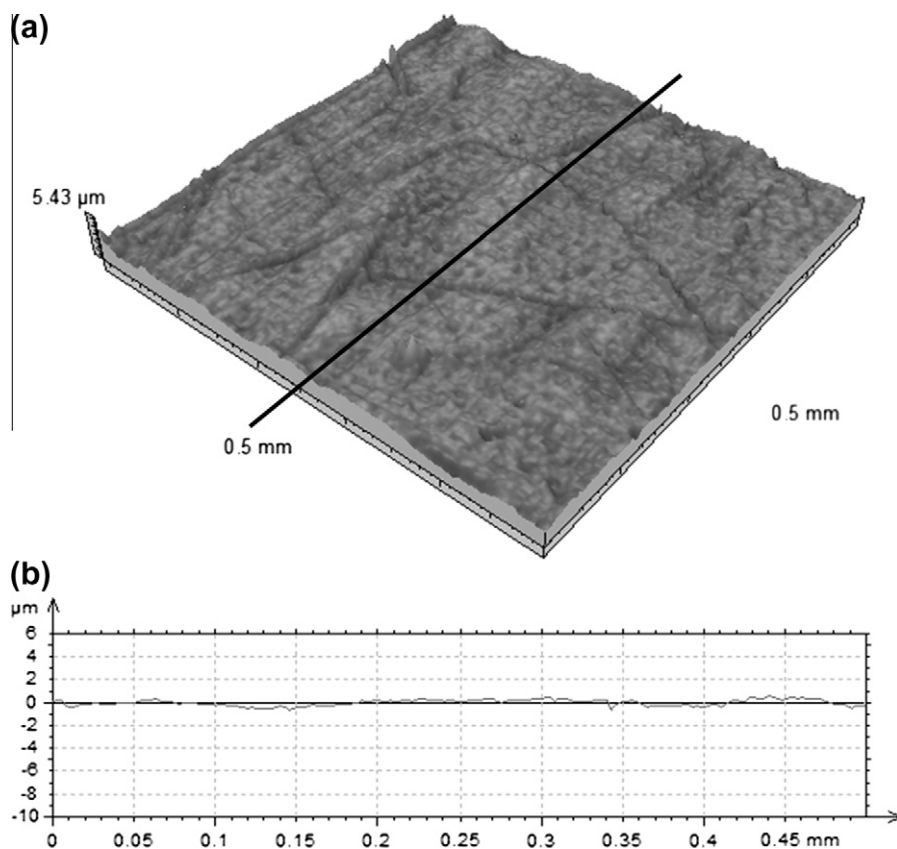


Fig. 3. Surface topography before plasma treatment. PS surface of sample 3A_p, as representative of surface topography of sample 3A_p, 4A_p, 6A_p and 7A_p. (a) 3D topography and (b) 2D profile (extracted at 50 mm from the edge of the square measured area).

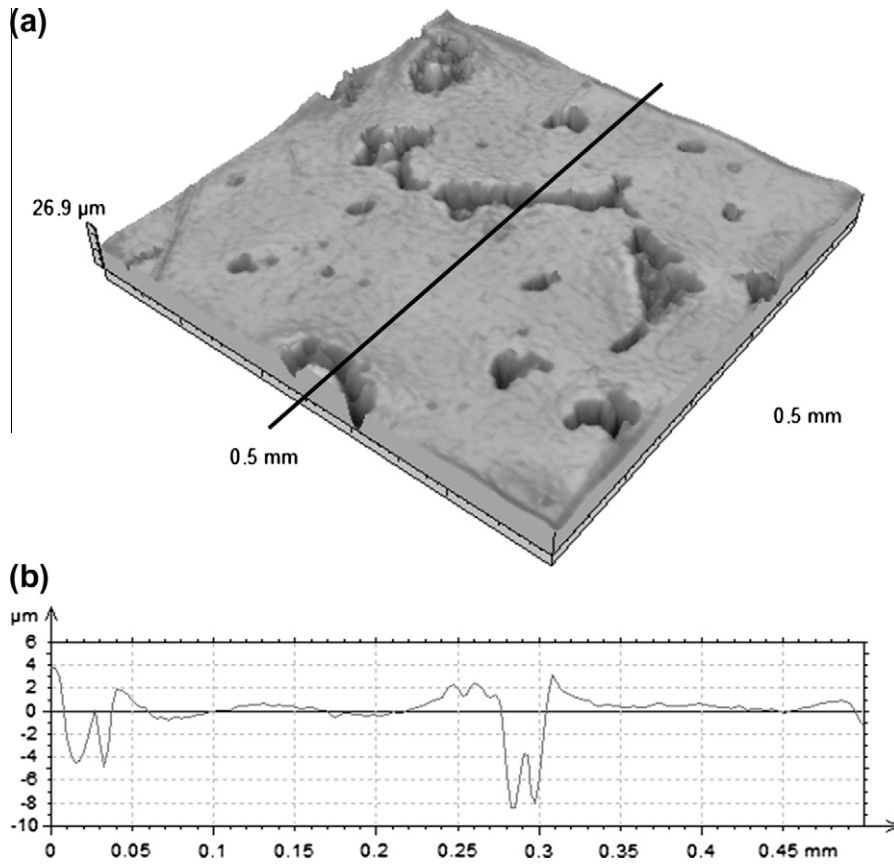


Fig. 4. Surface topography before plasma treatment. PS surface of sample 5A_p. (a) 3D topography and (b) 2D profile (extracted at 50 mm from the edge of the square measured area).

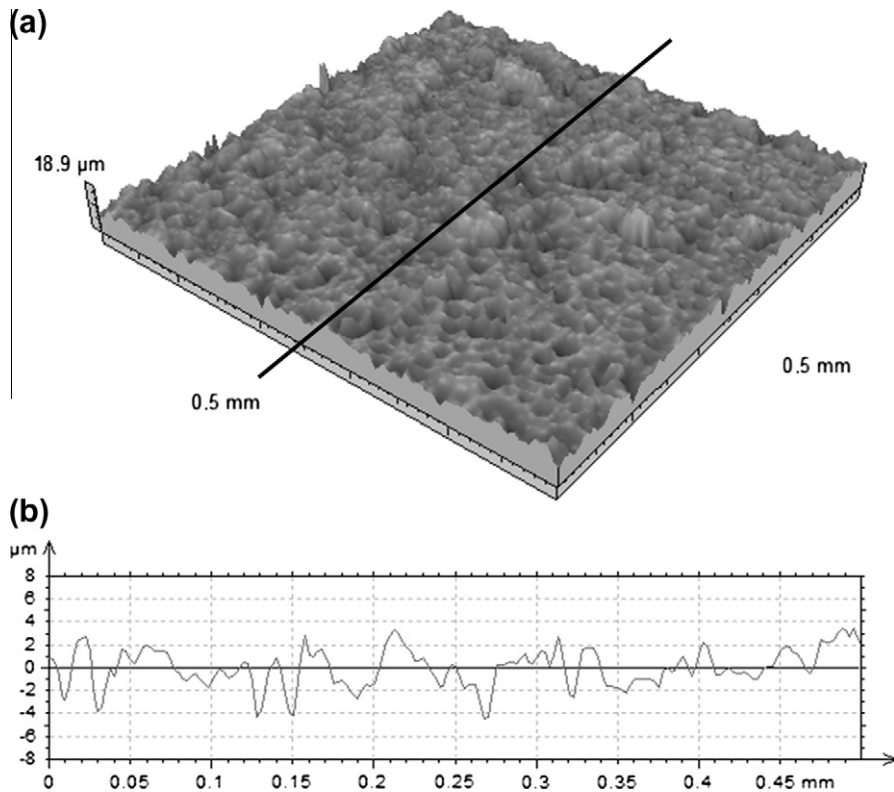


Fig. 5. Surface topography after plasma treatment. PS surface of sample 4B_p, as representative of surface topography of all plasma treated samples. (a) 3D topography and (b) 2D profile (extracted at 50 mm from the edge of the square measured area).

3. Results

3.1. Surface characterization

Table 1 summarizes the extracted roughness parameters from the profilometer whereas Fig. 1 shows the related FESEM images

(surface morphologies at the same magnification) of all PS materials. Figs. 2–4 show the plasma untreated PS surfaces, while Fig. 5 shows the typical topography of plasma treated samples. Fig. 6 shows the effects of thermoforming treatment through samples 1 and 4 considered as examples and Fig. 7 displays the profiles extracted at 50 mm from the edge of the square measured area.

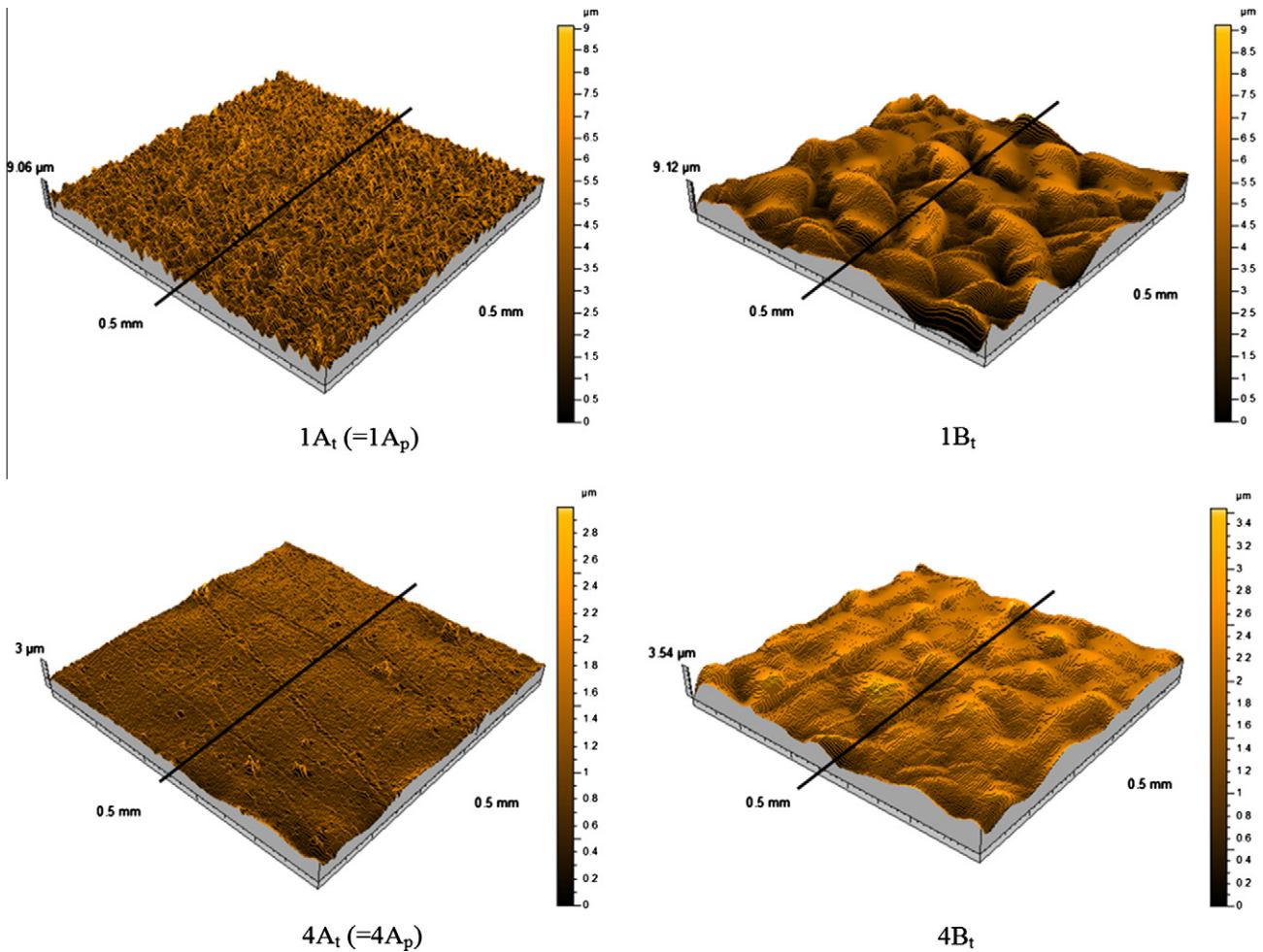


Fig. 6. 3D PS surface topography of sample 1 (up) and 4 (down), before (left) and after (right) thermoforming treatment.

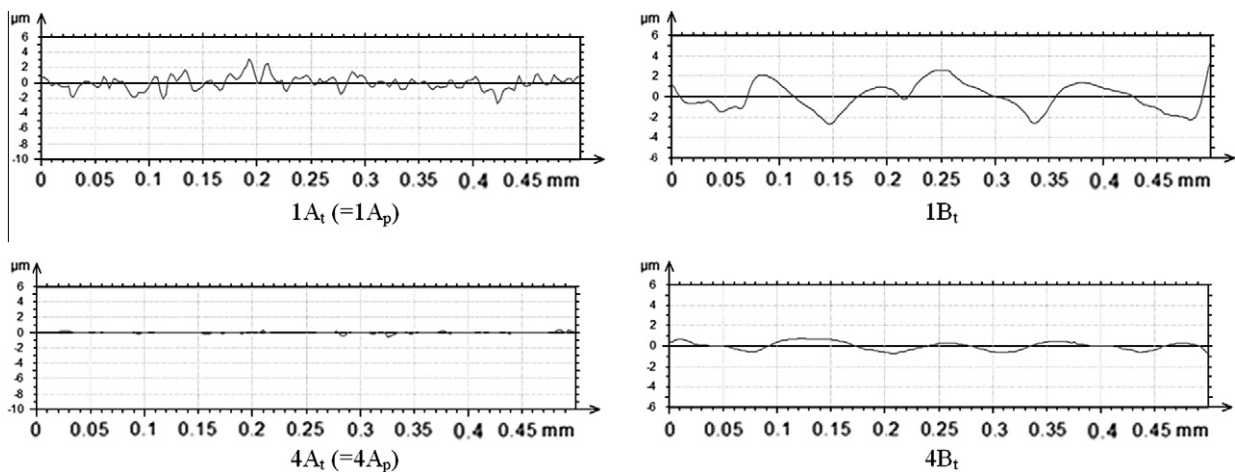


Fig. 7. 2D PS profiles of sample 1 (up) and 4 (down), before (left) and after (right) thermoforming treatment. Each profile was extracted at 50 mm from the edge of the square measured area shown in Fig. 6.

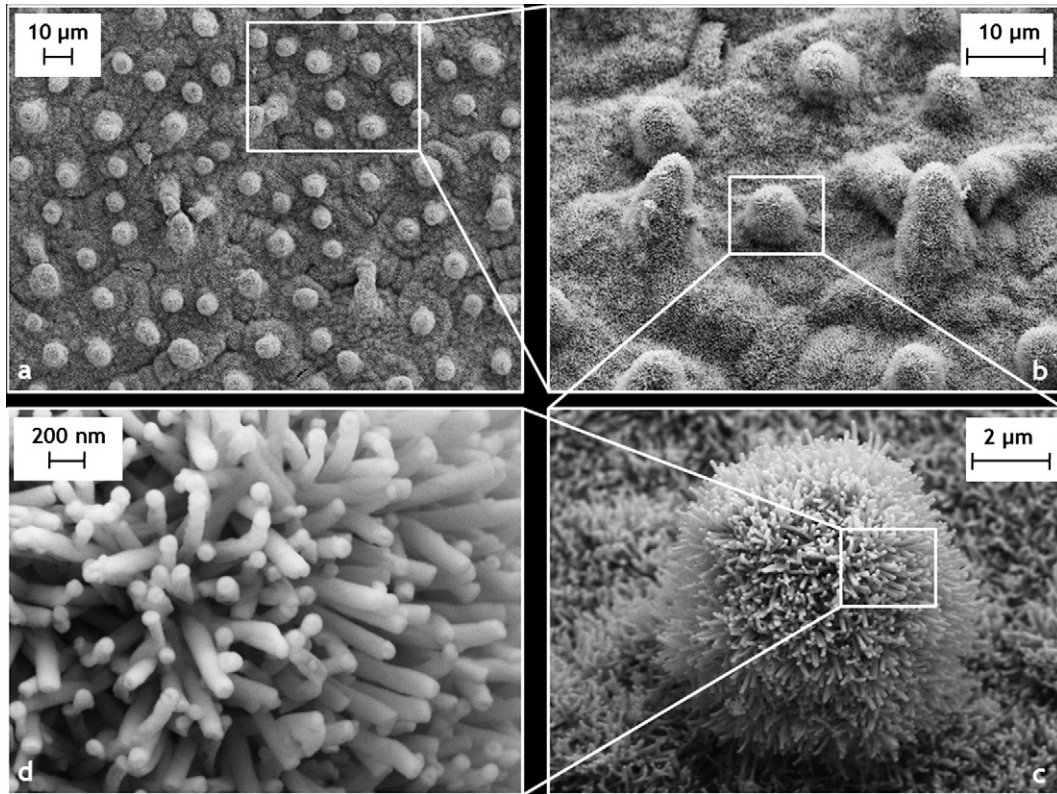


Fig. 8. FESEM microscopies of the lotus (*Nelumbo nucifera*) leaf: a natural 6-month dried adaxial leaf surface of lotus (a and b), the papillose cells (c) and the wax tubules (d).

Finally, the SEM morphology of the adaxial leaf surface of the water-repellent and self-cleaning lotus are reported in Fig. 8.

3.2. CA measurement

In Table 2, the mean values and standard deviation of 19 CA measurements for each PS surface are reported.

3.3. Sliding measurements

The results of the first applied procedure for the determination of sliding angle show that all PS surfaces have a sliding angle greater than 90° (no sliding). The exception is represented by the sample 4B_t, showing a sliding angle of 48 ± 15.7° (Fig. 9).

The sliding volume V_s and the sliding speed v_s for B_t surfaces were determined by means of the second procedure. The values

Table 2
CA measurements of all PS surfaces.

| | CA (°) |
|------------------------------------|----------|
| 1A _p = 1A _t | 55 ± 3.2 |
| 2A _p = 2A _t | 80 ± 5.8 |
| 3A _p = 3A _t | 72 ± 6.7 |
| 4A _p = 4A _t | 78 ± 7.6 |
| 5A _p = 5A _t | 69 ± 4.0 |
| 6A _p = 6A _t | 88 ± 3.8 |
| 7A _t | 89 ± 2.4 |
| 1B _p = 8A _t | 50 ± 6.7 |
| 2B _p = 9A _t | 84 ± 4.4 |
| 3B _p = 10A _t | 67 ± 3.3 |
| 4B _p = 11A _t | 50 ± 7.1 |
| 5B _p = 12A _t | 61 ± 6.1 |
| 6B _p = 13A _t | 87 ± 6.4 |
| 14A _t | 81 ± 2.8 |
| 7A _p | 78 ± 5.4 |
| 7B _p | 83 ± 5.0 |
| 1B _t | 93 ± 2.5 |
| 2B _t | 87 ± 3.7 |
| 3B _t | 81 ± 1.9 |
| 4B _t | 91 ± 4.2 |
| 5B _t | 82 ± 2.3 |
| 6B _t | 94 ± 2.8 |
| 7B _t | 88 ± 3.2 |
| 8B _t | 82 ± 2.4 |
| 9B _t | 89 ± 3.0 |
| 10B _t | 85 ± 5.0 |
| 11B _t | 84 ± 2.8 |
| 12B _t | 78 ± 4.4 |
| 13B _t | 77 ± 5.3 |
| 14B _t | 82 ± 1.9 |

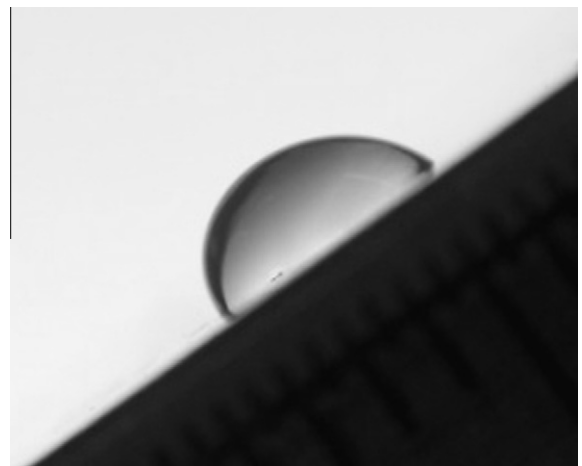


Fig. 9. Sample 4B_t at 36°, the sliding was observed at 48°.

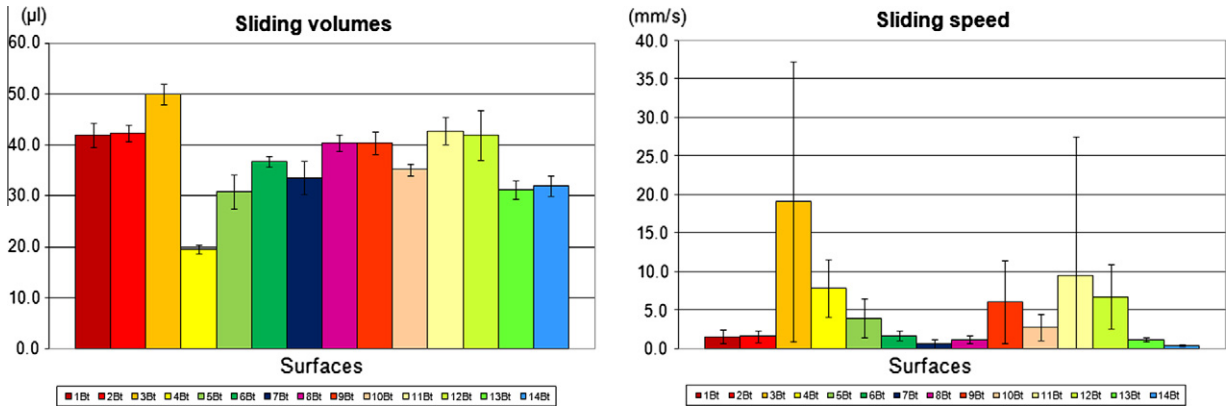


Fig. 10. Sliding volume or speed of B_t surfaces.

Table 3
Wenzel roughness parameters r of PS surfaces.

| | 1A _p | 2A _p | 3A _p | 4A _p | 5A _p | 6A _p | 7A _p |
|-------|-----------------|-----------------|-----------------|-----------------|-----------------|-----------------|-----------------|
| r_A | 1.0558 | 1.0528 | 1.0027 | 1.0011 | 1.1100 | 1.0006 | 1.0063 |
| | 1B _p | 2B _p | 3B _p | 4B _p | 5B _p | 6B _p | 7B _p |
| r_B | 1.2080 | 1.1450 | 1.0709 | 1.1297 | 1.0629 | 1.1166 | 1.1553 |

of V_s and v_s were calculated from five measurements per each sample, see Fig. 10.

4. Discussion

4.1. Plasma treatment

According to Wenzel $\cos \theta_{A,B} = r_{A,B} \cdot \cos \theta_{A,B}$, where $r_{A,B} = \frac{r_B}{r_A}$, r_A (1.0006–1.0558) and r_B (1.0629–1.2080) are the Wenzel roughness parameters (reported in Table 3), before or after the plasma treatment respectively, $\theta_{A,B}$ is the corresponding theoretical contact angle; thus, we could evaluate the effect of the plasma treatment by the increment of the superficial roughness. The comparison between theoretical predictions and experimental data is presented in Fig. 11.

According to the FESEM microscopies reported in Fig. 1, the plasma treatment increases the surface roughness. It is necessary to consider sample 5A_p separately, since it presents a specific initial (untreated, Fig. 4) situation showing several distributed valleys with greater depth than in other samples, thus implying the greatest value of the Sdr parameter (11%); after plasma treatment, the Sdr parameter is of the same order of magnitude as for the other samples (see Table 1). The plasma treatment levels the surface with deep valleys, as we can see in sample 5, and by surface erosion eliminates the presence of excessive high peaks. Except for sample 5, the plasma treatment increases the roughness parameters (see Sa, Sq, Sp, Sv, Sz in Table 1) leading to more valleys than peaks (negative value of Ssk) with a greater effective area than the untreated surfaces (greater value of Sdr). Apart from samples 2A_p and 7A_p, we observed a decrement of CA as expected from the

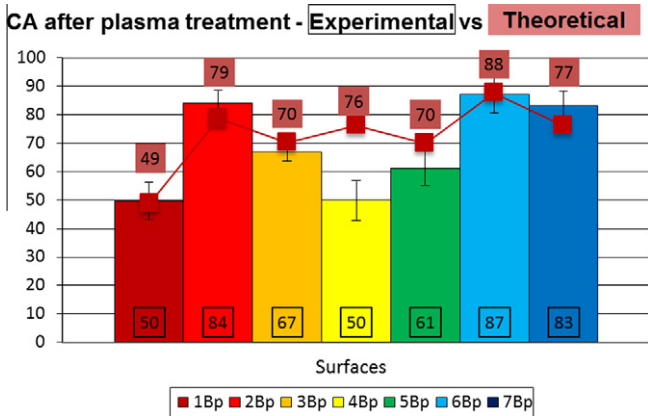


Fig. 11. Experimental measurements vs. theoretical predictions of CA for samples after plasma treatment.

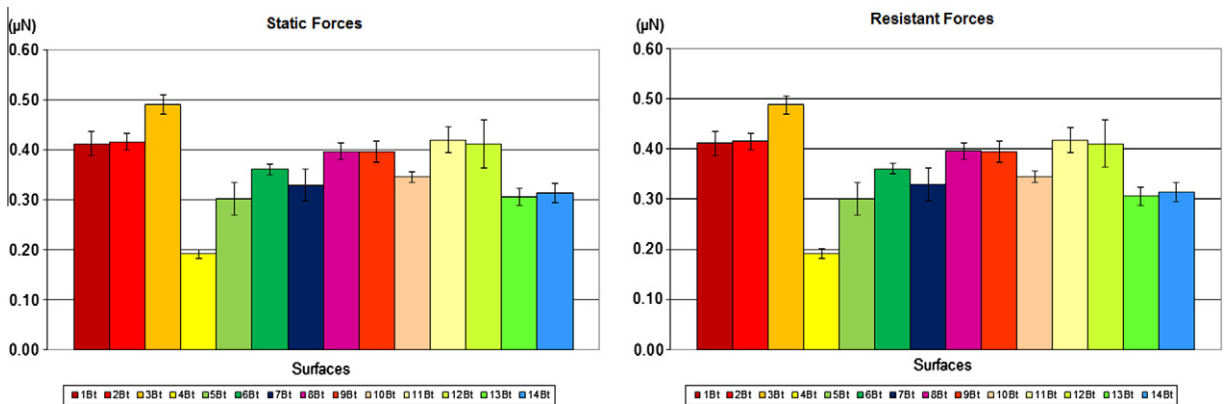


Fig. 12. Static and resistant forces on B_t surfaces.

Table 4

Contact angle, sliding angle, sliding volume and speed of a natural 6-month dried adaxial leaf surface of lotus.

| | Lotus (<i>Nelumbo nucifera</i>) |
|----------------------|-----------------------------------|
| CA (°) | 153.4 ± 3.28 |
| Sliding angle (°) | 26.2 ± 3.64 |
| Sliding volume (μl) | 4.7 ± 1.15 |
| Sliding speed (mm/s) | 233.3 ± 25.82 |
| Static force (μN) | 0.043 ± 0.008 |
| Resistant force (μN) | 0.032 ± 0.009 |

Wenzel theory for an intrinsically hydrophilic material subjected to an increment of roughness. Thus plasma treatment is ideal for increasing the PS surface wettability.

4.2. Thermoforming treatment: adhesive static and resistant forces

Considering the roughness parameters reported in Table 1 and the profilometer 3D-images of Fig. 6, we could observe that the thermoforming treatment globally decreases the roughness parameters (see Sa, Sq, Sp, Sv, Sz in Table 1). Referring to the Sdr parameter close to 0%, we can say that the thermoforming treatment renders the surfaces smoother. Apart from samples 13A_t, we observed an increment of the CA as expected from the Wenzel theory for an intrinsically hydrophilic material subjected to a decrement of the roughness.

Finally, we calculate the static and the resistant forces of sliding drops for B_t vertical (at 90°) surfaces (Fig. 12) and on a natural 6-month dried lotus leaf for comparison. The complete measured wettability parameters of lotus leaf are summarized in Table 4.

The static force (F_S) was computed as follows:

$$F_S = m \cdot g = V \cdot \rho_0 \cdot g \quad (1)$$

where V is the drop sliding volume, ρ_0 is water density and g is gravity acceleration. The resistant force (F_R) was obtained, assuming a resistant force during sliding on PS proportional to the low velocity observed, as:

$$F_R = F_S \cdot \left(1 - \frac{F_{RL}}{F_S} \frac{v}{v_{OL}}\right) \quad (2)$$

where F_S is the static force of the surface, F_{RL} and v_{OL} are the resistant force ($0.032 \pm 0.009 \mu\text{N}$) and the sliding speed ($233 \pm 25.82 \text{ mm/s}$) for the lotus leaf, respectively, and v is the sliding speed of the surface. The resistant force of the lotus leaf was computed as proportional to the velocity square, due to the high velocity observed:

$$F_{RL} = \frac{1}{2} \cdot \rho_0 \cdot v_{OL}^2 \cdot A_r \cdot C_p \quad (3)$$

where A_r is the resistant area ($2.32 \pm 0.327 \text{ mm}^2$) and C_p is drag coefficient (equal to ~ 0.47 since the shape of the sliding drop is nearly a sphere), finding $F_{RL} \approx 0.03 \mu\text{N}$. The resistance forces are found to be negligible, thus static and resistant force are nearly identical (Fig. 12).

5. Conclusions

In this paper the effects of plasma and thermoforming treatments on the water sliding behavior have been studied on 14 different PS surfaces, in terms of contact angle, sliding angle, sliding volume, sliding speed, and static and resistant forces acting on the sliding drop. We compared the experimental results with those on a natural 6-month dried lotus leaf. A significant correlation between technological treatment, surface roughness parameters and wetting measurements clearly emerges. Thus, the analysis sug-

gests that plasma/thermoforming are ideal treatments to tune the wettability and enhance the hydrophilic/hydrophobic behavior of PS surfaces.

Acknowledgments

The authors would like to thank M. Biasotto of the Department of Special Surgery and B. Codan of the Division of Dental Sciences and Biomaterials of the Department of Biomedicine at the University of Trieste for their help in using the surface profilometer. The authors wish to sincerely thank A. Chiodoni, Physical Department, Politecnico di Torino for the fundamental help performing the FES-EM micrographs of A_p, B_p and A_t samples and lotus leaf. The authors thank James Vanzo for the final English grammar supervision. NMP is supported by “Metrology on a cellular and macromolecular scale for regenerative medicine” – metregen (2009–2012).

References

- [1] Barthlott W. Epidermal and seed surface characters of plants: systematic applicability and some evolutionary aspects. *Nord J Bot* 1981;1:345–55.
- [2] Neinhuis C, Barthlott W. Characterization and distribution of water-repellent, self-cleaning plant surfaces. *Ann Bot* 1997;79:667–77.
- [3] Barthlott W, Neinhuis C. Purity of the sacred lotus, or escape from contamination in biological surfaces. *Planta* 1997;202:1–8.
- [4] Herminghaus S. Roughness induced non-wetting. *Europhys Lett* 2000;52:165–70.
- [5] Wagner P, Furstner R, Barthlott W, Neinhuis C. Quantitative assessment to the structural basis of water repellency in natural and technical surfaces. *J Exp Bot* 2003;385:1295–303.
- [6] Nosonovsky M, Bhushan B. Roughness optimization for biomimetic superhydrophobic surfaces. *Microsyst Technol* 2005;11:535–49.
- [7] Lu-quan R, Shu-jie W, Xi-mei T, Zhi-wu H, Lin-na Y, Zhao-mei Q. Non-smooth morphologies of typical plant leaf surfaces and their anti-adhesion effects. *J Bionic Eng* 2007;4:33–40.
- [8] Otten A, Herminghaus S. How plants keep dry: a physicists point of view. *Langmuir* 2004;20:2405–8.
- [9] Zhiqing Y, Hong C, Jianxin T, Huifang G, Yuejun L, Zhengxiang W, et al. A novel preparation of polystyrene film with a superhydrophobic surface using a template method. *J Phys D Appl Phys* 2007;40:3485–9.
- [10] Brushan B, Jung YC. Wetting, adhesion and friction of superhydrophobic and hydrophilic leaves and fabricated micro/nanopatterned surfaces. *J Phys Condens Matter* 2008;20:225010 (24pp).
- [11] Solga A, Cerman Z, Striffler BF, Spaeth M, Barthlott W. The dream of staying clean: lotus and biomimetic surfaces. *Bioinsp Biomim* 2007;2:126–34.
- [12] Young T. An essay on the cohesion of fluids. *Phil Trans Roy Soc* 1805;95:65–87.
- [13] Wenzel RN. Resistance of solid surfaces to wetting by water. *Ind Eng Chem* 1936;28:988–94.
- [14] Cassie ABD, Baxter S. Wettability of porous surfaces. *Trans Faraday Soc* 1944;40:546–51.
- [15] Pugno NM. Towards a Spiderman suit: large invisible cables and self-cleaning releasable superadhesive materials. *J Phys Condens Matter* 2007;39:395001 (17pp).
- [16] Pugno NM. The Nanomechanics in Italy, Research signpost (IND); 2007.
- [17] Bosia F, Pugno N, Buehler M. Hierarchical simulations for the design of super-tough nanofibres inspired by spider silk. *Phys Rev E* 2010;82:056103 (7pp).
- [18] Bignardi C, Petraroli M, Pugno N. Nanoindentations on conch shells of Gastropoda and Bivalvia molluscs reveal anisotropic evolution against external attacks. *J Nanosci Nanotechnol* 2010;10:6453–60.
- [19] Pugno N. Mimicking nares width super-nanotubes for producing optimized super-composites. *Nanotechnology* 2006;17:5480–4.
- [20] Pugno N, Carpinteri A. Design of micro-nanoscale bio-inspired hierarchical materials. *Philos Mag Lett* 2008;88:397–405.
- [21] Pugno N, Bosia F, Carpinteri A. Multiscale stochastic simulations for tensile testing of nanotube-based macroscopic cables. *Small* 2008;4:1044–52.
- [22] Burton Z, Bhushan B. Hydrophobicity, adhesion and friction properties of nanopatterned polymers and scale dependence for MEMS/NEMS. *Nano Lett* 2005;5:1607–13.
- [23] Bhushan B, Jung YC. Wetting study of patterned surfaces for superhydrophobicity. *Ultramicroscopy* 2007;107:1033–41.
- [24] Bhushan B, Nosonovsky M, Jung YC. Towards optimization of patterned superhydrophobic surfaces. *J Roy Soc Interface* 2007;4:643–8.
- [25] Jung YC, Bhushan B. Contact angle, adhesion and friction properties of micro- and nanopatterned polymers for superhydrophobicity. *Nanotechnology* 2006;17:4970–80.
- [26] Jung YC, Bhushan B. Wetting transition of water droplets on superhydrophobic patterned surfaces. *Scr Mater* 2007;57:1057–60.
- [27] Nosonovsky M, Bhushan B. Wetting of rough three-dimensional superhydrophobic surfaces. *Microsyst Technol* 2006;12:273–81.

- [28] Nosonovsky M, Bhushan B. Hierarchical roughness makes superhydrophobic states stable. *Microelectron Eng* 2007;84:382–6.
- [29] Shibuichi S, Onda T, Satoh N, Tsujii K. Super-water-repellent surfaces resulting from fractal structure. *J Phys Chem* 1996;100:19512–7.
- [30] Hozumi A, Takai O. Preparation of silicon oxide films having a water-repellent layer by multiple-step microwave plasma-enhanced chemical vapor deposition. *Thin Solid Films* 1998;334:54–9.
- [31] Miwa M, Nakajima A, Fujishima A, Hashimoto K, Watanabe T. Effects of the surface roughness on sliding angles of water droplets on superhydrophobic surfaces. *Langmuir* 2000;16:5754–60.
- [32] Oner D, McCarthy TJ. Ultrahydrophobic surfaces. Effects of topography length scales on wettability. *Langmuir* 2000;16:7777–82.
- [33] Lau KKS, Bico J, Teo KBK, Chhowalla M, Amaratunga GAJ, Milne WL, et al. Superhydrophobic carbon nanotube forests. *Nano Lett* 2003;3:1701–5.
- [34] Quéré D. Fakir droplets. *Nat Mater* 2002;1:14–5.
- [35] Noeske M, Degenhardt J, Strudhoff S, Lommattzsch U. Plasma jet treatment of five polymers at atmospheric pressure: surface modifications and the relevance for adhesion. *Int J Adhes Adhes* 2004;2:171–7.
- [36] Valeri S, Paradisi P, Luches P, Bona A. Growth and morphology of Te films on Mo. *Thin Solid Films* 1999;352:114–8.
- [37] Bellucci S, Bergamaschi A, Bottini M, Magrini A, Mustelin T. Biomedical platforms based on composite nanomaterials and cellular toxicity. *J Phys* 2007;61:95–8.
- [38] Lepore E, Antonioli F, Brianza S, Buono M, Carpinteri A, Pugno N. Preliminary in vivo experiments on adhesion of geckos. *J Nanomaterials* 2008;2008:194524 (5 pp).
- [39] Pugno NM, Lepore E. Living tokay geckos display adhesion times following Weibull statistics. *J Adhes* 2008;84:949–62.
- [40] Pugno NM, Lepore E. Observation of optimal gecko's adhesion on nanorough surfaces. *Biosystems* 2008;94:218–22.
- [41] Adamson AV. *Physical chemistry of surfaces*. NY: Wiley; 1990.
- [42] Israelachvili JN. *Intermolecular and surface forces*. 2nd ed. London: Academic press; 1992.
- [43] Brushan B. *Principles and applications of tribology*. NY: Wiley; 1999.
- [44] Brushan B. *Introduction to tribology*. NY: Wiley; 2002.